ASTROBIOLOGY
Volume 22, Number 3, 2022

DOI: 10.1089/ast.2021.0053

Research Articles

Open camera or QR reader and scan code to access this article and other resources online.

Radiolytic Destruction of Uracil in Interstellar and Solar System Ices

Perry A. Gerakines,[1,i] Danna Qasim,[1–3,ii] Sarah Frail,[1,4] and Reggie L. Hudson[1,iii]

Abstract

Uracil is one of the four RNA nucleobases and a component of meteoritic organics. If delivered to the early Earth, uracil could have been involved in the origins of the first RNA-based life, and so this molecule could be a biomarker on other worlds. Therefore, it is important to understand uracil's survival to ionizing radiation in extraterrestrial environments. Here we present a study of the radiolytic destruction kinetics of uracil and mixtures of uracil diluted in H_2O or CO_2 ice. All samples were irradiated by protons with an energy of 0.9 MeV, and experiments were performed at 20 and 150 K to determine destruction rate constants at temperatures relevant to interstellar and Solar System environments. We show that uracil is destroyed much faster when H_2O ice or CO_2 ice is present than when these two ices are absent. Moreover, destruction is faster for CO_2-dominated ices than for H_2O-dominated ones and, to a lesser extent, at 150 K compared with 20 K. Extrapolation of our laboratory results to astronomical timescales shows that uracil will be preserved in ices with half-lives of up to $\sim 10^7$ years on cold planetary bodies such as comets or Pluto. An important implication of our results is that for extraterrestrial environments, the application of laboratory data measured for the radiation-induced destruction of pure (neat) uracil samples can greatly underestimate the molecule's rate of destruction and significantly overestimate its lifetime, which can lead to errors of over 1000%. Key Words: Astrochemistry—Ice chemistry—Nucleobases—Radiolysis—Cosmic rays—Uracil. Astrobiology 22, 233–241.

1. Introduction

Organic molecules, including biologically relevant ones, have been detected in meteorites, in cometary dust and comae, on planetary surfaces, in planetary atmospheres, toward protostars, in protoplanetary disks, and in cold cores of the interstellar medium (ISM) (*e.g.*, Elsila *et al.*, 2009; Callahan *et al.*, 2011; Mumma and Charnley, 2011; McGuire, 2018; Altwegg *et al.*, 2019). Understanding the origins and evolution of extraterrestrial organics, such as amino acids and nucleobases, may provide clues to the origins of the chemistry involved in terrestrial biological activity and guide searches for biomarkers in extraterrestrial environments.

Uracil is an RNA nucleobase that is not found in DNA and differs from DNA's thymine by a single methyl group (Fig. 1). Uracil is one of the nucleobases identified in organic material extracted from meteorites, including Murchison, Murray, and Orgueil (Stoks and Schwartz, 1979), which suggests that uracil may be formed in space. A uracil precursor, urea (Davidson and Baudisch, 1926), also has been extracted from meteorite samples (Hayatsu *et al.*, 1975) and has been identified in the ISM by Belloche *et al.* (2019) and Jiménez-Serra *et al.* (2020). In addition to this evidence for extraterrestrial uracil, this molecule's interstellar formation has been investigated through experimental and theoretical studies. Such work includes

[1]Astrochemistry Laboratory, NASA Goddard Space Flight Center, Greenbelt, Maryland, USA.
[2]Department of Physics and Astronomy, Howard University, Washington, District of Columbia, USA.
[3]Center for Research and Exploration in Space Science and Technology, NASA/GSFC, Greenbelt, Maryland, USA.
[4]Department of Biochemistry, Stanford University School of Medicine, Stanford, California, USA.
[i]ORCID ID (https://orcid.org/0000-0002-9667-5904).
[ii]ORCID ID (https://orcid.org/0000-0002-3276-4780).
[iii]ORCID ID (https://orcid.org/0000-0003-0519-9429).

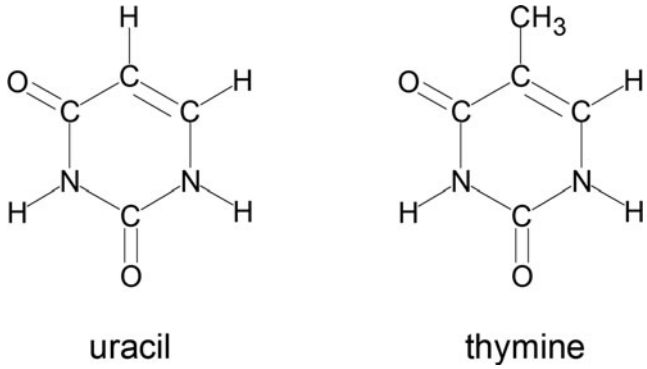

FIG. 1. Structures of uracil and thymine.

uracil's synthesis in interstellar ice analogs (*e.g.*, Materese *et al.*, 2013) and in the gas phase (Wang and Bowie, 2012).

The detection of uracil and other nucleobases is important for searches for the signatures of life on planetary surfaces. Europa, for example, is the subject of various exploration missions and is suspected to have a potentially habitable subsurface ocean (Reynolds *et al.*, 1983). Such an ocean, coupled with vertical transport of material, could mean that Europa might have biomarkers on its surface. However, like many objects and regions in space, Europa is exposed to ionizing radiation that can destroy organic molecules. Understanding the lifetimes of organics and potential biomarkers subjected to radiation is thus important for interpreting observations that indicate their presence or absence in a radiation-rich environment.

Even though it has been shown that uracil can be formed in a radiation environment, the balance of formation and destruction due to radiation must also be considered, especially when evaluating uracil as a possible biomarker. Many studies of uracil's photo- and radiation chemistry are in the literature, covering this molecule as a room temperature neat solid, in a room temperature liquid solution, and frozen in an aqueous solution. Among many examples are studies by Wang (1961), Smith (1963), Varghese (1971), Shragge *et al.* (1974), Shetlar and Basus (2011), Saïagh *et al.* (2015), and Rouquette *et al.* (2020). Most such work focused on the identification of room temperature reaction products, typically with chromatographic methods, as opposed to studying the molecule's destruction kinetics or stability. Peeters *et al.* (2003) used a different approach, examining the photolytic destruction of uracil in solid argon as a way to judge the molecule's gas-phase lifetime in the ISM. Examples of radiation-chemical studies of uracil destruction include those by Pilling *et al.* (2011) with X-rays and Hammer *et al.* (2019) with γ rays, both being studies of uracil at room temperature.

Despite this rich history of work on uracil, several areas remain to be studied. In this article, we investigate the radiation-chemical destruction of uracil-containing ices, with all measurements being made *in situ*. Three possible influences on uracil destruction in ices are studied. First, we compare one-component samples (*i.e.*, neat uracil) and two-component ices, dominated by either CO_2 or H_2O. Second, we vary uracil's concentration in our two-component samples, examining a wide range of mixing ratios in each case. Third, we report results for two ice temperatures, 20 and 150 K, which are relevant to the ISM and the outer Solar System, to evaluate temperature effects on uracil's destruction. In all cases, our focus is on determination of rate constants and half-lives for uracil's radiolytic destruction, with reaction products only briefly addressed. With our rate constants and associated half-lives, we are able to predict uracil's stability in various astronomical environments. The work presented here is a continuation of our study of the radiolytic destruction of amino acids and nucleobases (Gerakines *et al.*, 2012; Gerakines and Hudson, 2013, 2015; Materese *et al.*, 2020).

2. Experimental Methods

The equipment and techniques used for this study have been described by Gerakines and Hudson (2013) and Materese *et al.* (2020). Briefly, ices were created in a high-vacuum chamber ($P \sim 2–5\times10^{-7}$ Torr with the system at room temperature and $P \sim 5\times10^{-8}$ Torr when cold) on a polished aluminum substrate (area $\approx 5\,cm^2$), which was mounted on the cold finger of a closed-cycle helium cryostat ($T_{min} \sim 20$ K). Ice temperatures were measured with a silicon diode sensor attached to the substrate, and a resistive heater was used to reach and control temperatures above 20 K. The vacuum chamber was interfaced with a beamline from a Van de Graaff accelerator that produced ~ 0.9 MeV protons. Infrared (IR) spectra of ices were obtained with a Nicolet Nexus 670 spectrometer coupled to the vacuum chamber, with the IR beam reflected from the sample surface at $\sim 15°$ from a line drawn perpendicular to the substrate. Spectra were recorded as the average of 100 scans from 5000 to $650\,cm^{-1}$. The spectral resolution was $1\,cm^{-1}$ for the CO_2 + uracil ices and $4\,cm^{-1}$ for samples of uracil and H_2O + uracil.

Uracil was sublimated from a custom-made Knudsen-type oven located inside the vacuum chamber, as used by Gerakines *et al.* (2012) for making samples containing amino acids. The oven consisted of a copper block with a small cavity ($\sim 0.05\,cm^3$) that held the uracil powder. A copper plate with a small hole (diameter ≈ 1 mm) covered the sample. A 100-Ω heater, silicon diode, and controller were used to set and maintain the temperature of the oven near 180°C, where uracil sublimation was sufficient to produce samples at a reasonable rate for these experiments. Thermal degradation of uracil is not expected at temperatures below 245°C (see, *e.g.*, Maddern *et al.*, 2016), and no evidence of degradation was observed in our IR spectra of deposited uracil.

To create ice mixtures, H_2O vapor or CO_2 gas was introduced into the vacuum chamber from a separate gas manifold through a metered flow valve as the uracil was sublimated from the oven. The flow valve was calibrated to yield the desired mixing ratios for the ice samples. Ice thicknesses were monitored by laser interferometry during growth. Deposition times were dictated by the rate of uracil sublimation from the oven, which typically resulted in an increase in the resulting sample's thickness of $\sim 1.0\,\mu m\,h^{-1}$. Deposition rates of mixtures (gas + uracil) usually resulted in ice growth rates of 2.5 to $60\,\mu m\,h^{-1}$, depending on the desired mixing ratio. Thicknesses of the irradiated samples ranged from 1.3 to 5 μm. Given the amount of H_2O background gas in our system when cold ($\sim 5\times10^{-8}$ Torr), the

contamination levels in the two neat uracil samples are estimated to be less than 2%, and for all other samples, they are less than 0.8%.

The compounds used in this study were uracil (99% purity; Sigma Chemical Co), CO_2 (99.99% purity; Aldrich Chemical Co.), and ultrapure H_2O with a resistivity greater than 18.2 MΩ cm, obtained by a reverse osmosis system. Liquid H_2O was degassed with three freeze–pump–thaw cycles before each use. The uracil and H_2O + uracil samples were deposited at 150 K, cooled to 20 K if necessary, and then irradiated. The CO_2 + uracil mixtures were deposited at 50 K, to avoid the sublimation that would occur at higher temperatures, and then cooled to 20 K and irradiated. Both sets of ice mixtures included samples with matrix-to-uracil molar ratios of 10:1, 30:1, 100:1, and 270:1.

To irradiate ices, samples were positioned to face our accelerator's proton beam, with the beam current being measured as ∼150 nA. The radiation dose was calculated as follows:

$$\text{Dose(MGy)} = SF \times (1.602 \times 10^{-22}) \quad (1)$$

where S is the ice sample's proton stopping power (in eV cm^2 g^{-1} $p+^{-1}$), F is the proton fluence (in p^+ cm^{-2}) as determined from the integrated current through the sample, and the factor of 1.602×10^{-22} converts dose units from eV g^{-1} to MGy. Table 1 lists the proton stopping powers for our samples, which we calculated using the Stopping and Range of Ions in Matter (SRIM) software package from Ziegler *et al.* (2010). The density of each two-component sample, which was needed for calculation of S, was estimated as the weighted average of the two components. The densities used were 1.617 g cm^{-3} for uracil (Parry, 1954), 0.93 g cm^{-3} for H_2O ice (Brown *et al.*, 1996), and 1.67 g cm^{-3} for CO_2 (Loeffler *et al.*, 2016). Protons were incident over the full surface area of the samples (∼5 cm^2).

3. Results

The IR spectrum we obtained for uracil at 20 K is shown at the bottom of Fig. 2. This spectrum agrees with published data taken at room temperature. For example, the atlas of Pouchert (1997) has a spectrum of uracil as a nujol mull and, like ours, it shows pronounced absorption at 3500 to 2500, 1700 to 1600, 1500 to 1400, and near 1220 cm^{-1}. The same can be said for room temperature IR spectra of solid uracil from studies by Saïagh *et al.* (2015) and Rouquette *et al.* (2020). Other examples from the literature include uracil spectra from studies by Angell (1961), Susi and Ard (1971), Barnes *et al.* (1984), Aamouche *et al.* (1996), and Rozenberg *et al.* (2004).

Table 1. Properties of Ice Samples

Sample	*Mixing ratio*	*Stopping power, S/10⁸ eV cm² g⁻¹ p+⁻¹*	*Density, ρ/g cm⁻³*
Uracil	—	2.471	1.617
CO_2 + uracil	10:1	2.278	1.665
	30:1	2.254	1.668
	100:1	2.243	1.669
	270:1	2.240	1.670
H_2O + uracil	10:1	2.602	0.99
	30:1	2.645	0.95
	100:1	2.669	0.94
	270:1	2.677	0.93

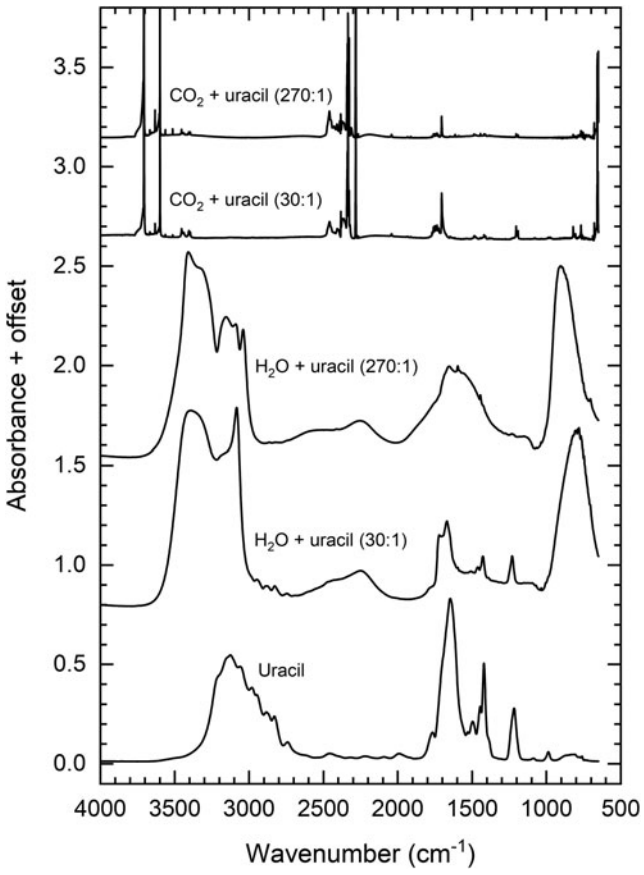

FIG. 2. IR spectra of uracil, H_2O + uracil, and CO_2 + uracil at 20 K. Note that the strongest absorption features of CO_2 are too intense to fit on this scale. Sample thicknesses were 1.3–5 μm, depending on the mixture.

For details of assignments of specific IR features of uracil, see the articles already cited, particularly by Rozenberg *et al.* (2004). In short, the intense, broad IR absorption of uracil from about 3500 to 2500 cm^{-1} in the bottom spectrum of our Fig. 2 is due to various C-H and N-H stretching vibrations, while bending, double-bond stretches, and deformations dominate from about 2000 to 1000 cm^{-1}. These same IR bands are also found in the spectra of H_2O + uracil and CO_2 + uracil mixtures recorded at 20 K, with mixing ratios of 30:1 and 270:1. Again, see Fig. 2.

We studied the radiation-induced destruction of solid uracil by following changes in its IR spectrum with increasing radiation dose. With ices made only of uracil (*i.e.*, neat samples) and in H_2O + uracil experiments, we monitored destruction using the IR band at 1217 cm^{-1}, which was both sharp and relatively free of overlap with other IR features. However, for CO_2 + uracil experiments, we monitored uracil's sharp IR feature at 1646 cm^{-1}. Distortions and spectral interference were increasingly problematic with the higher matrix-to-uracil ratios, as can be seen by comparing Fig. 2's spectra of the H_2O + uracil 30:1 and 270:1 samples, the result being that we were unable to carry out accurate measurements at ratios above 270:1.

The IR spectra of the CO_2 + uracil (30:1) and H_2O + uracil (30:1) ice mixtures irradiated at 20 K are presented in Fig. 3. In the CO_2 + uracil samples, known radiolysis products of solid CO_2 were observed (*e.g.*, Bennett *et al.*, 2004), including CO (2140 cm^{-1}), CO_3 (2044, 1881, 1071, and 974 cm^{-1}), and O_3 (1046 cm^{-1}). In our H_2O + uracil experiments, the radiation products identified were similar to those reported by Materese *et al.* (2020) for thymine, as expected, and include HNCO (2251 cm^{-1}), OCN^- (2171 cm^{-1}), CO_2 (2341 cm^{-1}), and CO (2140 cm^{-1}). The IR bands of HNCO and OCN^- were not seen in the CO_2 + uracil experiments, suggesting that H_2O is required for their formation or that H_2O ice might be better at preserving HNCO and OCN^- in the sample. Unassigned IR features were found at 1292 and 1333 cm^{-1} after irradiation.

Uracil destruction in our experiments was quantified with the methods used in our studies of amino acids and thymine (Gerakines *et al.*, 2012; Gerakines and Hudson, 2013, 2015; Materese *et al.*, 2020). The relative abundance of uracil was determined after each irradiation step by measuring the area (A) of either the 1217 or 1646 cm^{-1} band. Figure 4 shows the resulting trend of the surviving fraction (A/A_0) of uracil with radiation dose (D) for each sample. The data were analyzed assuming reversible first-order kinetics as

$$\text{Uracil} \rightleftharpoons \text{Products}, \tag{2}$$

with forward and reverse rate constants denoted by k_1 and k_{-1}, respectively. With this model, we fit the data using

$$(A/A_0) = ae^{-bD} + c, \tag{3}$$

where the initial band area (A_0) is proportional to uracil's initial abundance and a, b, and c are independent parameters. The best-fitting sets of a, b, and c are listed in Table 2 and curve fits are shown in Fig. 4. The analytical solution of this simple kinetic model gives the mathematical relationship between these parameters and the reaction rate constants (Gerakines and Hudson, 2013, and references therein). Parameter a corresponds to $k_1/(k_1 + k_{-1})$, which can also be written as $\left(1 - \frac{A_\infty}{A_0}\right)$, where A_∞ is the relevant band's area at chemical equilibrium. Similarly, b corresponds to the sum of the rate constants, $k_1 + k_{-1}$, and c is uracil's equilibrium fraction $\frac{A_\infty}{A_0}$, which can also be written in terms of the rate constants as $k_{-1}/(k_1 + k_{-1})$. In each ice mixture studied, the destruction rate constant was calculated by using $k_1 = ab$.

Equation 3 was used to fit the kinetic data we obtained for uracil mixtures, but was not used for the neat uracil samples, where the surviving fraction remained above ~88% for absorbed doses up to 40 MGy, as seen in Fig. 4a. The plots of surviving fraction versus dose at both 20 and 150 K cover only the initial uracil destruction, which is approximately linear. Because of this, the data for irradiation of uracil at 20 and 150 K were fit with a line. Mathematically, we note that if $bD << 1$, Eq. 3 approximates to $(a + c) - bD$. Since our experiments only cover uracil's initial decay, linear fits to the data in Fig. 4a gave the values of b in Table 2 for the neat uracil samples. Values of the parameters a and c could not be determined in these cases but are constrained by their definitions in the analytical solution to be less than or equal to 1.

The uracil half-life dose in each ice also was determined, representing the radiation dose needed to reduce uracil's abundance by 50%. We then used the results to estimate uracil's half-life in various astronomical environments, where the radiation dose rates are known or estimated. Table 3 lists the destruction rate constants and half-life doses for each experiment, and Fig. 5 shows the trends in k_1 with temperature and ice composition. For neat uracil samples, only an upper limit to k_1 could be determined since the fit parameter a is unknown in those cases. It should be noted that while the CO_2 + uracil and H_2O + uracil mixtures are not realistic representations of the composition of mixtures in space (partly due to experimental limitations), our

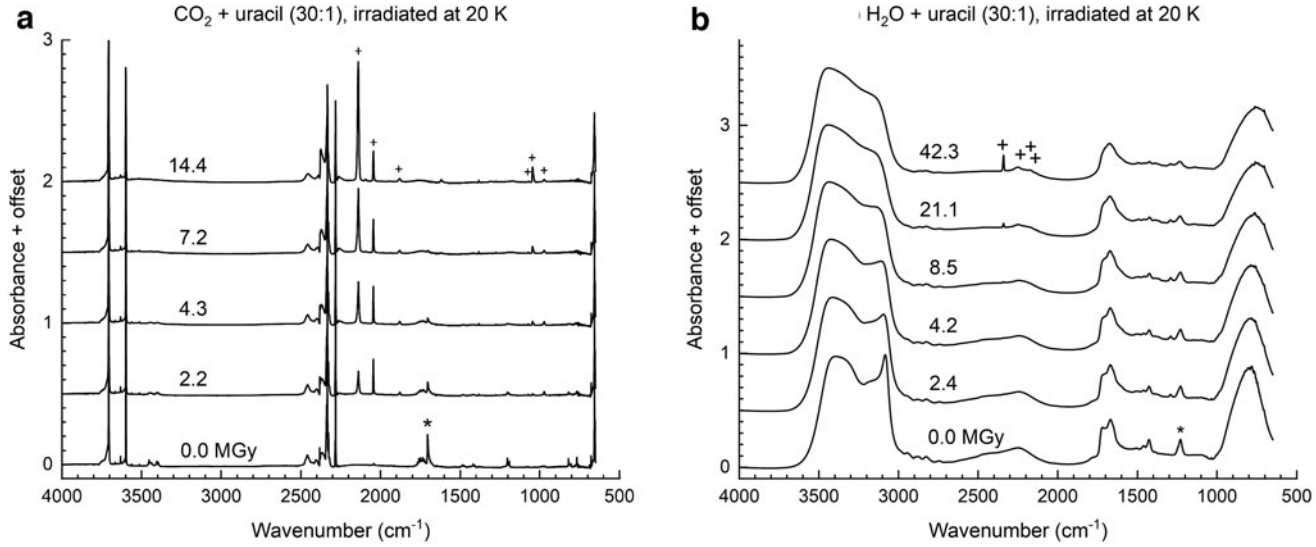

FIG. 3. IR spectra of **(a)** CO_2 + uracil (30:1) and **(b)** H_2O + uracil (30:1) samples before and after irradiation at 20 K. Spectra are labeled according to the total radiation dose absorbed by the sample, in units of MGy. Asterisks (*) mark uracil features used to measure the destruction kinetics, and plus signs (+) indicate IR features of radiation products.

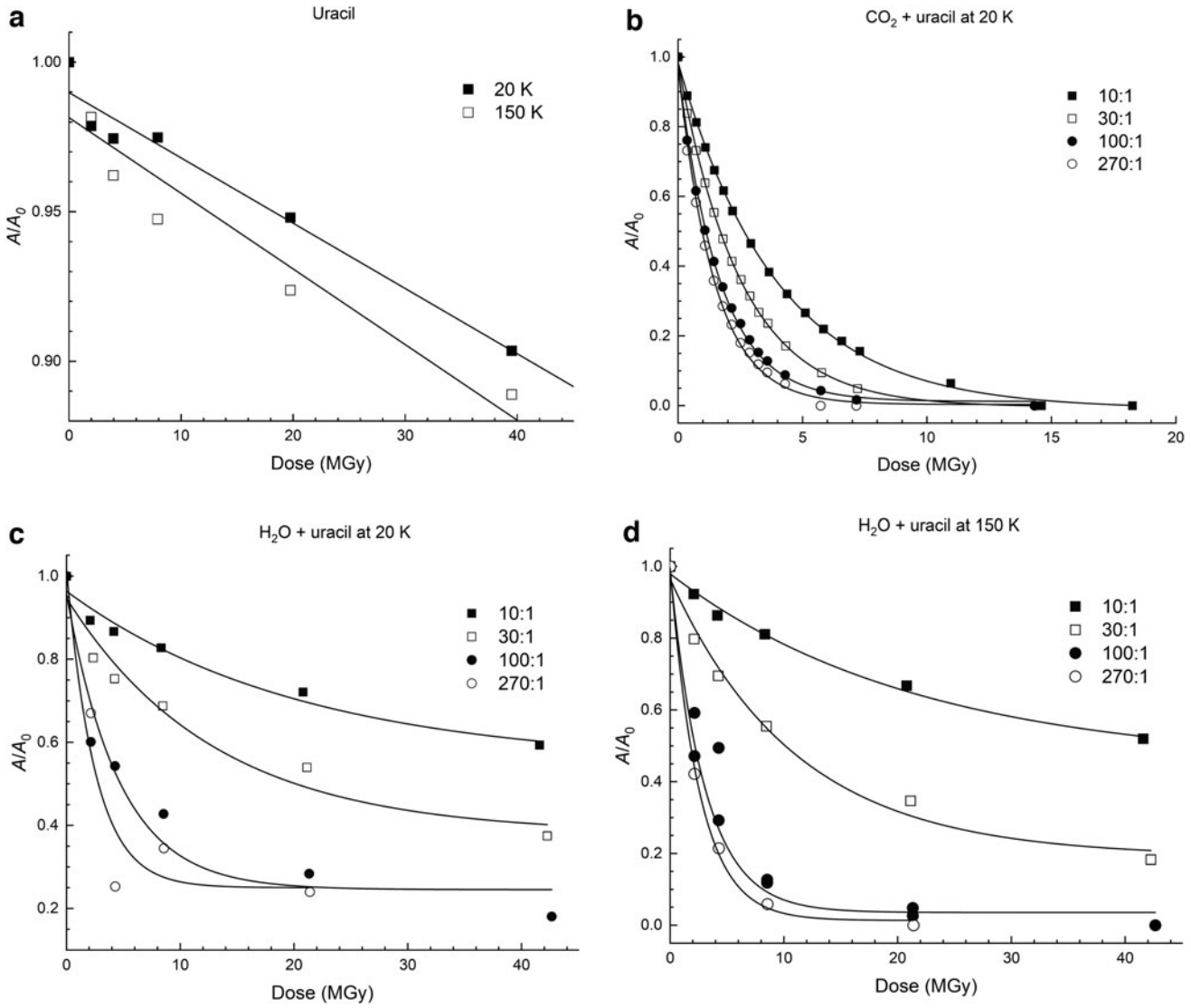

FIG. 4. Surviving fraction of uracil versus dose in radiation experiments involving **(a)** uracil samples at 20 and 150 K, **(b)** CO_2 + uracil mixtures irradiated at 20 K, **(c)** H_2O + uracil mixtures irradiated at 20 K, and **(d)** H_2O + uracil mixtures irradiated at 150 K. All plots include the fits described in the text and Table 2.

results should represent the general behavior of uracil when diluted in ices dominated by CO_2 or H_2O. If necessary, the trends in Fig. 5 could be extrapolated to uracil ices of lower concentration.

4. Discussion

4.1. Radiolytic destruction of uracil

Figure 5 and Table 3 illustrate the influence of ice composition on the radiolytic destruction of uracil. We first note that the destruction rate constant is considerably smaller in neat uracil than in the two-component mixtures. For the mixtures, uracil's destruction rate constant is higher in CO_2-dominated ice than in H_2O-dominated ice, a trend also observed with glycine-containing ices by Gerakines and Hudson (2013, 2015). As discussed by Gerakines and Hudson (2015), at least two factors contribute to this behavior. One is the outcome of indirect radiolytic action, in which the matrix strongly influences the observed chemical changes. For example, CO_2 destruction gives CO + O, and O is highly reactive. Ozone (O_3) is also a radiolysis product of CO_2, as confirmed from the IR data, and can aid in uracil's destruction.

Another trend shown in Fig. 5a is that the destruction rate constant increases with the mixing ratio (*i.e.*, lower uracil concentration) in both CO_2 + uracil and H_2O + uracil samples. This same trend was found for amino acids and thymine by Gerakines *et al.* (2012), Gerakines and Hudson (2013, 2015), and Materese *et al.* (2020). With higher mixing ratios, more of the reactive intermediates from irradiated CO_2 or H_2O are available to combine with uracil, but in ices with smaller amounts of CO_2 or H_2O, more of the uracil is directly affected by irradiation, and the reaction products may simply recombine. Consistent with this idea, slopes of the destruction rate constant curves in Fig. 5 decrease with increasing mixing ratio as the radiation products of CO_2 or H_2O will increasingly interact with each other instead of with uracil.

Table 2. Curve-Fit Parameters for Uracil Destruction

Ice sample	*Mixing ratio*	*T/K*	*Curve-fit parameters*[a]		
			a	b/*MGy*$^{-1}$	c
Uracil	—	20	—	0.0021 ± 0.0001[b]	—
	—	150	—	0.0024 ± 0.0004[b]	—
CO_2 + uracil	10:1	20	0.99 ± 0.01	0.252 ± 0.004	0.0090 ± 0.0056
	30:1	20	0.99 ± 0.01	0.40 ± 0.01	-0.003 ± 0.005
	100:1	20	0.96 ± 0.01	0.61 ± 0.02	0.012 ± 0.008
	270:1	20	0.97 ± 0.01	0.69 ± 0.02	0.0035 ± 0.0087
H_2O + uracil	10:1	20	0.42 ± 0.08	0.049 ± 0.022	0.55 ± 0.08
	30:1	20	0.57 ± 0.08	0.077 ± 0.030	0.38 ± 0.08
	100:1	20	0.71 ± 0.09	0.22 ± 0.07	0.26 ± 0.06
	270:1	20	0.77 ± 0.16	0.40 ± 0.20	0.25 ± 0.10
	10:1	150	0.53 ± 0.05	0.046 ± 0.011	0.45 ± 0.06
	30:1	150	0.77 ± 0.05	0.091 ± 0.017	0.19 ± 0.05
	100:1	150	0.97 ± 0.05	0.25 ± 0.03	0.018 ± 0.032
	270:1	150	0.98 ± 0.03	0.39 ± 0.03	0.013 ± 0.017

[a]With the exception of the uracil data, fits are in the form of Eq. 3.
[b]Linear fit to $A/A_0 = (a + c) - bD$. Only b could be determined independently. See text.

Figure 5 also shows how temperature influences uracil's radiolytic destruction. For H_2O + uracil ices, there is only a slight increase in the destruction rate constant when comparing irradiation at 20 and 150 K (a similar trend was observed for glycine by Gerakines and Hudson, 2015). The measured increase of k_1 with T is likely due to the increased mobility of the remaining radiation products at higher temperatures. Contrary to this idea, Materese *et al.* (2020) found that the destruction rate constant of thymine decreased as the irradiation temperature increased. However, most of the thymine-containing ice samples in that study were grown in an amorphous form, as opposed to the mostly crystalline form in this study. It is possible that the ice's structure (whether amorphous or crystalline) may influence the destruction rate constants of uracil as well, but this was not studied here.

One goal of the present work on uracil and our previous article on thymine (Materese *et al.*, 2020) is to compare the resistance of nucleobases to ionizing radiation. From Table 3 and our earlier article, we have the following half-life doses:

> 40 MGy—20 K, uracil;
38 MGy—13 K, thymine;
4.8 MGy—20 K, H_2O + uracil (100:1);
4.3 MGy—13 K, H_2O + thymine (50:1);
2.8 MGy—150 K, H_2O + uracil (100:1); and
8.0 MGy—100 K, H_2O + thymine (50:1).

The temperature and composition are not perfectly matched, but we feel confident in suggesting from such comparisons that the half-life doses are not substantially different between uracil and thymine. This is not surprising given the similarities in structures of the two molecules, as shown in Fig. 1.

Comparisons with results on the radiation-induced destruction of uracil from elsewhere are somewhat difficult due to differences in experimental conditions. Hammer *et al.* (2019) found little destruction of neat uracil after γ irradiation with doses in the 0–1 MGy range, which matches the small changes in our Fig. 4a. A destruction half-life of 2×10^7 years for uracil in dense molecular clouds was reported by Pilling *et al.* (2011) from X-irradiation of neat

Table 3. Destruction Rate Constants and Half-Life Doses for Uracil in Ice Mixtures

Ice sample	*Mixing ratio*	*T/K*	*Destruction rate constant* k_1/*MGy*$^{-1}$	*Half-life dose/MGy*
Uracil	—	20	<0.0021[a]	>40
Uracil	—	150	<0.0024[a]	>40
CO_2 + uracil	10:1	20	0.25 ± 0.01	2.79 ± 0.07
	30:1	20	0.39 ± 0.01	1.69 ± 0.04
	100:1	20	0.58 ± 0.02	1.12 ± 0.05
	270:1	20	0.67 ± 0.02	0.97 ± 0.05
H_2O + uracil	10:1	20	0.02 ± 0.01	>40
	30:1	20	0.04 ± 0.02	20.2 ± 11.5
	100:1	20	0.16 ± 0.05	4.8 ± 1.9
	270:1	20	0.3 ± 0.2	2.8 ± 1.8
	10:1	150	0.025 ± 0.007	50.5 ± 27.4
	30:1	150	0.07 ± 0.01	10.13 ± 2.6
	100:1	150	0.25 ± 0.03	2.8 ± 0.5
	270:1	150	0.38 ± 0.03	1.8 ± 0.2

[a]Due to the fitting process, only an upper limit could be obtained (see text and Table 2).

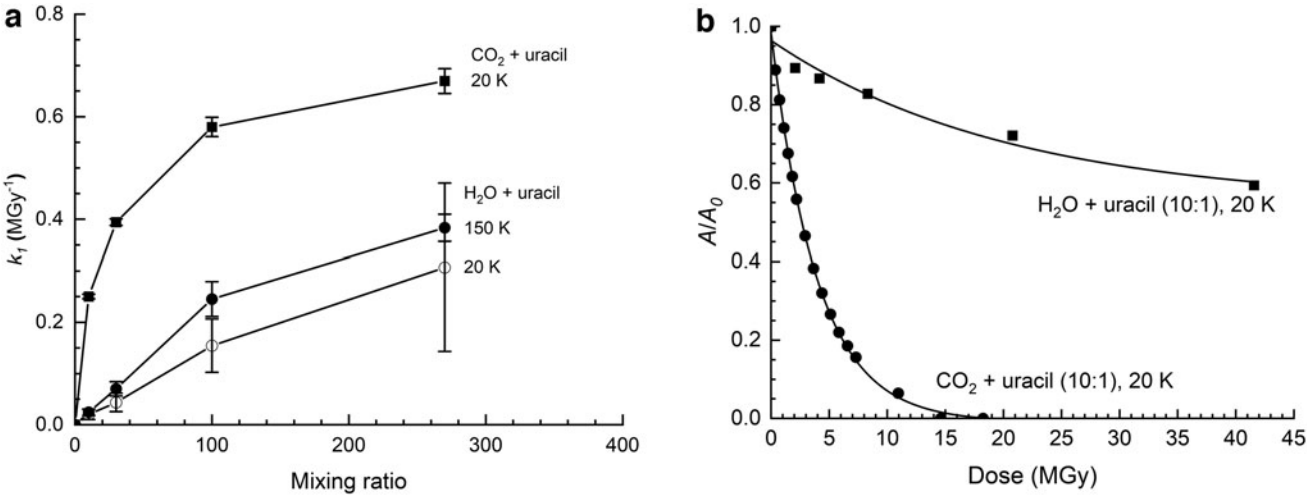

FIG. 5. Comparisons of the radiolytic destruction of uracil at 20 K in CO_2 and in H_2O. **(a)** Dependence of the uracil destruction rate constant k_1 on the ice mixing ratio. **(b)** Decay curves of uracil as a function of the absorbed dose for the 10:1 mixtures at 20 K.

uracil near 298 K. However, our (Table 3) results suggest that this value is about 10^3 times higher than for uracil irradiated in the presence of H_2O ice and at more relevant interstellar temperatures.

4.2. Astrobiological applications

We applied the half-life doses for uracil in Table 3 to Solar System objects and interstellar clouds to determine survival times for uracil in those environments, and the results are presented in Table 4. Since uracil is likely to be far less abundant than H_2O or CO_2 in space, data for the most dilute samples (*i.e.*, those with a mixing ratio of 270:1) were used to derive the results in Table 4. Moreover, the samples with the closest temperature to the relevant environment were chosen (either 20 K or 150 K). Note that for the dense ISM, H_2O is observed primarily in amorphous form, so the results for our samples created at 150 K may require some adjustment. However, based on our results, at any temperature and for any mixing ratio, uracil is more likely to be preserved in H_2O ice than in CO_2 ice in all astronomical environments.

Because dense interstellar clouds begin to gravitationally collapse after 10^4–10^5 years and are expected to have lifetimes of about 10^7 years (Herbst and Klemperer, 1973), a uracil half-life of only $\sim 10^4$ years in dense clouds is relatively short. Thus, the transfer of uracil ice directly from a cloud to the next stages in the star formation cycle (*e.g.*, protoplanetary disks or planetesimals) may not be likely if uracil is formed early in the cloud's life. However, as shown in Table 4, the extrapolated half-life of uracil in comets at 1 cm depth is tens of millions of years and therefore comets are a promising means of delivering interstellar uracil to the inner Solar System. There is substantial evidence from the recent Rosetta mission to comet 67P/Churyumov–Gerasimenko that comets can supply a large fraction of organics to the young Earth (*e.g.*, Marty *et al.*, 2017; Altwegg *et al.*, 2019). Additionally, ice reaction chemistry can continue in the mid-planes of protoplanetary disks and

TABLE 4. RADIOLYTIC HALF-LIVES OF URACIL IN VARIOUS ASTRONOMICAL ENVIRONMENTS BASED ON THE RESULTS FOR CO_2 + URACIL AND H_2O + URACIL (270:1) MIXTURES

Location	*T/K*	*Depth/cm*	*Dose rate/Gy years^{-1}*	*Half-life in CO_2/year*	*Half-life in H_2O/year*
Mars[a]	200	0	1.8×10^{-1}	$(5.6\pm0.3)\times10^{6}$	$(1.0\pm0.1)\times10^{7}$
		100	1.0×10^{-1}	$(9.5\pm0.5)\times10^{6}$	$(1.8\pm0.2)\times10^{7}$
Europa[b]	100	10^{-3}	1.1×10^{7}	$(8.9\pm0.5)\times10^{-3}$	$(1.7\pm0.2)\times10^{-1}$
		1	1.3×10^{4}	$(7.3\pm0.4)\times10^{1}$	$(1.4\pm0.2)\times10^{2}$
		100	2.2	$(4.5\pm0.2)\times10^{5}$	$(8.3\pm0.9)\times10^{5}$
Pluto[c]	40	10^{-4}	1.3×10^{-1}	$(7.3\pm0.4)\times10^{6}$	$(2.1\pm1.4)\times10^{7}$
		100	3.9×10^{-2}	$(2.5\pm0.1)\times10^{7}$	$(7.2\pm4.6)\times10^{7}$
Comets[d]	40	10^{-4}	6.0	$(1.6\pm0.08)\times10^{5}$	$(4.7\pm3.0)\times10^{5}$
		1	4.6×10^{-2}	$(2.1\pm0.1)\times10^{7}$	$(6.1\pm3.9)\times10^{7}$
Dense ISM[e]	10	—	1.2×10^{2}	$(8.0\pm0.4)\times10^{3}$	$(2.3\pm1.5)\times10^{4}$
Diffuse ISM[e]	40	—	6.0×10^{5}	1.6 ± 0.1	4.7 ± 3.0

[a]Dartnell *et al.* (2007), fig. 3; absorbed dose for pure ice.
[b]Paranicas *et al.* (2009), fig. 9; dose rate includes protons and electrons.
[c]Hudson *et al.* (2008), table 1.
[d]Strazzulla *et al.* (2003), fig. 6; dose time at 85 AU.
[e]Moore *et al.* (2001), table 1; dose rate includes UV photons and protons.
ISM, interstellar medium.

interstellar material can play an important role in such disk chemistry, meaning that uracil ice has the potential to be formed again in disks. In addition, as a planetary disk evolves, meteorite parent bodies experience hydrothermal processing, which can potentially form complex molecules such as uracil or amino acids (Kebukawa *et al.*, 2017).

Within the Solar System, uracil's survival depends strongly on the environment, where molecules exposed on planetary surfaces may be strongly affected by UV photons. For example, uracil exposed on the surface of Mars is unlikely to survive more than $\sim 10^7$ years. However, minerals on Mars can shield uracil from harsh radiation (*e.g.*, Ertem *et al.*, 2017), and lakes or ice located beneath the martian surface (*e.g.*, Lauro *et al.*, 2021) may also preserve uracil. In these cases, our survival half-lives should be adjusted to reflect the shielding effects, which have not been studied here. Europa's surface is reported to be $\sim$10–100 million years old (Ip *et al.*, 1998), which is significantly younger than that of Mars. The high radiation dose rate of $\sim 10^7$ Gy yr^{-1} at a depth of 0.01 mm on Europa would destroy uracil with a half-life of just 2 months. However, Europa is thought to have an ocean beneath its icy surface and active resurfacing could occur (*e.g.*, Squyres *et al.*, 1983). Pluto, on the other hand, is reported to have a surface less than 10 million years old (Trilling, 2016) and even as young as $\sim 10^5$ years (Buhler and Ingersoll, 2018). Evidence for organic molecules has been seen both on Pluto's surface and in its tenuous atmosphere (Cruikshank *et al.*, 2019). With an estimated half-life of $\sim 10^7$ years, any uracil delivered to Pluto's surface may be present in detectable amounts.

In closing, we again note and emphasize that our rate constants for destruction of uracil in ice mixtures, with either H_2O or CO_2 present, are orders of magnitude larger than for neat uracil samples. Extrapolations to astronomical environments of laboratory data on radiation-induced destruction of uracil alone (without the effects of the ice matrix) can greatly underestimate the molecule's rate of destruction and significantly overestimate its extraterrestrial lifetime, leading to errors of over 1000%.

5. Conclusions

The destruction of uracil and uracil in CO_2 or H_2O ice mixtures by proton irradiation was experimentally investigated at temperatures relevant to the ISM and the Solar System. From the IR data collected, radiation products identified included CO, CO_3, and O_3 for uracil mixed with CO_2, and HNCO, OCN^-, CO_2, and CO for uracil mixed with H_2O. Destruction rate constants of uracil (and thus uracil's survivability in each case) were found to depend on ice composition and uracil concentration, where CO_2 + uracil mixtures were found to possess the highest destruction rate constants (and lowest uracil survivability). To a lesser extent, the irradiation temperature (20 or 150 K) influenced uracil's destruction rate constants, where higher destruction was observed at higher temperatures. Half-life doses were determined and used to evaluate the survival of uracil in various extraterrestrial environments in the absence of shielding effects. Our results suggest that uracil has its greatest chance of survival on or beneath the surfaces of icy objects, such as comets or Pluto.

Author Disclosure Statement

No competing financial interests exist.

Funding Information

The NASA Astrobiology Institute supported this work through funding awarded to the Goddard Center for Astrobiology under proposal 13-13NAI7-0032, which also provided a summer fellowship to S.F. Support is also acknowledged from the NASA-GSFC FLaRe ISFM Program and from NASA CRESST, award number 80GSFC21M0002. Early financial support came from NASA's Exobiology Program. Marla Moore (NASA, retired) assisted with our experiments.

References

Aamouche A, Ghomi M, Coulombeau C, *et al.* (1996) Neutron inelastic scattering, optical spectroscopies and scaled quantum mechanical force fields for analyzing the vibrational dynamics of pyrimidine nucleic acid bases. 1. Uracil. *J Phys Chem* 100:5224–5234.

Altwegg K, Balsiger H, and Fuselier SA (2019) Cometary chemistry and the origin of icy solar system bodies: the view after Rosetta. *Annu Rev Astron Astrophys* 57:113–155.

Angell CL (1961) Infrared spectroscopic investigation of nucleic acid constituents. *J Chem Soc* 504–515.

Barnes AJ, Stuckey MA, and Legall L (1984) Nucleic-acid bases studied by matrix-isolation vibrational spectroscopy—uracil and deuterated uracils. *Spectrochim Acta A* 40:419–431.

Belloche A, Garrod RT, Muller HSP, *et al.* (2019) Re-exploring molecular complexity with alma (ReMoCa): interstellar detection of urea. *Astron Astrophys* 628:1–62.

Bennett CJ, Jamieson C, Mebel AM, *et al.* (2004) Untangling the formation of the cyclic carbon trioxide isomer in low temperature carbon dioxide ices. *Phys Chem Chem Phys* 6:735–746.

Brown DE, George SM, Huang C, *et al.* (1996) H_2O condensation coefficient and refractive index for vapor-deposited ice from molecular beam and optical interference measurements. *J Phys Chem* 100:4988–4995.

Buhler PB and Ingersoll AP (2018) Sublimation pit distribution indicates convection cell surface velocities of similar to 10 cm per year in Sputnik Planitia, Pluto. *Icarus* 300:327–340.

Callahan MP, Smith KE, Cleaves HJ, *et al.* (2011) Carbonaceous meteorites contain a wide range of extraterrestrial nucleobases. *Proc Natl Acad Sci U S A* 108:13995–13998.

Cruikshank DP, Materese CK, Pendleton YJ, *et al.* (2019) Prebiotic chemistry of Pluto. *Astrobiology* 19:831–848.

Dartnell LR, Desorgher L, Ward JM, *et al.* (2007) Modelling the surface and subsurface Martian radiation environment: implications for astrobiology. *Geophys Res Lett* 34:1–6.

Davidson D and Baudisch O (1926) The preparation of uracil from urea. *J Am Chem Soc* 48:2379–2383.

Elsila JE, Glavin DP, and Dworkin JP (2009) Cometary glycine detected in samples returned by Stardust. *Meteorit Planet Sci* 44:1323–1330.

Ertem G, Ertem MC, Mckay CP, *et al.* (2017) Shielding biomolecules from effects of radiation by Mars analogue minerals and soils. *Int J Astrobiol* 16:280–285.

Gerakines PA and Hudson RL (2013) Glycine's radiolytic destruction in ices: first in situ laboratory measurements for mars. *Astrobiology* 13:647–655.

Gerakines PA and Hudson RL (2015) The radiation stability of glycine in solid CO_2- in situ laboratory measurements with applications to Mars. *Icarus* 252:466–472.

Gerakines PA, Hudson RL, Moore MH, *et al.* (2012) In situ measurements of the radiation stability of amino acids at 15–140 K. *Icarus* 220:647–659.

Hammer PG, Yi RQ, Yoda I, *et al.* (2019) Radiolysis of solid-state nitrogen heterocycles provides clues to their abundance in the early Solar System. *Int J Astrobiol* 18:289–295.

Hayatsu R, Studier MH, Moore LP, *et al.* (1975) Purines and triazines in Murchison meteorite. *Geochim Cosmochim Acta* 39:471–488.

Herbst E and Klemperer W (1973) Formation and depletion of molecules in dense interstellar clouds. *Astrophys J* 185:505–533.

Hudson RL, Palumbo ME, Strazzulla G, *et al.* (2008) Laboratory studies of the chemistry of transneptunian object surface materials. In: *The Solar System Beyond Neptune*, edited by MA Barucci, H Boehnhardt, DP Cruikshank, and A Morbidelli, University of Arizona Press, Tucson, pp 507–523.

Ip WH, Williams DJ, McEntire RW, *et al.* (1998) Ion sputtering and surface erosion at Europa. *Geophys Res Lett* 25:829–832.

Jiménez-Serra I, Martin-Pintado J, Rivilla VM, *et al.* (2020) Center for Astrobiology: toward the RNA world in the interstellar medium-detection of urea and search of 2-aminooxazole and simple sugars. *Astrobiology* 20:1048–1066.

Kebukawa Y, Chan QHS, Tachibana S, *et al.* (2017) One-pot synthesis of amino acid precursors with insoluble organic matter in planetesimals with aqueous activity. *Sci Adv* 3:1–7.

Lauro SE, Pettinelli E, Caprarelli G, *et al.* (2021) Multiple subglacial water bodies below the south pole of Mars unveiled by new MARSIS data. *Nat Astron* 5:63–70.

Loeffler MJ, Moore MH, and Gerakines PA (2016) The effects of experimental conditions on the refractive index and density of low-temperature ices: solid carbon dioxide. *Astrophys J* 827:1–7.

Maddern TM, Jamier V, Brunton JR, *et al.* (2016) A technique to determine the thermal stability of uracil and uracil derivatives in a molecular beam. *Int J Mass Spectrom* 409:73–80.

Marty B, Altwegg K, Balsiger H, *et al.* (2017) Xenon isotopes in 67P/Churyumov-Gerasimenko show that comets contributed to Earth's atmosphere. *Science* 356:1069–1072.

Materese CK, Gerakines PA, and Hudson RL (2020) The radiation stability of thymine in solid H_2O. *Astrobiology* 20:956–963.

Materese CK, Nuevo M, Bera PP, *et al.* (2013) Thymine and other prebiotic molecules produced from the ultraviolet photo-irradiation of pyrimidine in simple astrophysical ice analogs. *Astrobiology* 13:948–962.

McGuire BA (2018) 2018 census of interstellar, circumstellar, extragalactic, protoplanetary disk, and exoplanetary molecules. *Astrophys J Suppl Ser* 239:1–48.

Moore MH, Hudson RL, and Gerakines PA (2001) Mid- and far-infrared spectroscopic studies of the influence of temperature, ultraviolet photolysis and ion irradiation on cosmic-type ices. *Spectrochim Acta A* 57:843–858.

Mumma MJ and Charnley SB (2011) The chemical composition of comets-emerging taxonomies and natal heritage. *Annu Rev Astron Astrophys* 49:471–524.

Paranicas C, Cooper JF, Garrett HB, *et al.* (2009) Europa's radiation environment and its effects on the surface. In: *Europa*, edited by RT Pappalardos, University of Arizona Press, Tucson, AZ, pp 529–544.

Parry GS (1954) The crystal structure of uracil. *Acta Crystallogr* 7:313–320.

Peeters Z, Botta O, Charnley SB, *et al.* (2003) The astrobiology of nucleobases. *Astrophys J* 593:L129–L132.

Pilling S, Andrade DPP, do Nascimento EM, *et al.* (2011) Photostability of gas- and solid-phase biomolecules within dense molecular clouds due to soft x-rays. *Mon Not R Astron Soc* 411:2214–2222.

Pouchert CJ (1997) *The Aldrich Library of FT-IR Spectra*. Aldrich Chemical Company, Milwaukee, WI.

Reynolds RT, Squyres SW, Colburn DS, *et al.* (1983) On the habitability of Europa. *Icarus* 56:246–254.

Rouquette L, Stalport F, Cottin H, *et al.* (2020) Dimerization of uracil in a simulated Mars-like UV radiation environment. *Astrobiology* 20:1363–1376.

Rozenberg M, Shoham G, Reva I, *et al.* (2004) Low temperature Fourier transform infrared spectra and hydrogen bonding in polycrystalline uracil and thymine. *Spectrochim Acta A* 60: 2323–2336.

Saïagh K, Cottin H, Aleian A, *et al.* (2015) VUV and mid-UV photoabsorption cross sections of thin films of guanine and uracil: application on their photochemistry in the Solar System. *Astrobiology* 15:268–282.

Shetlar MD and Basus VJ (2011) The photochemistry of uracil: a reinvestigation. *Photochem Photobiol* 87:82–102.

Shragge PC, Varghese AJ, Hunt JW, *et al.* (1974) Radiolysis of uracil in absence of oxygen. *Radiat Res* 60:250–267.

Smith KC (1963) Photochemical reactions of thymine, uracil, uridine, cytosine and bromouracil in frozen solution and in dried films. *Photochem Photobiol* 2:503–517.

Squyres SW, Reynolds RT, Cassen PM, *et al.* (1983) Liquid water and active resurfacing on Europa. *Nature* 301:225–226.

Stoks PG and Schwartz AW (1979) Uracil in carbonaceous meteorites. *Nature* 282:709–710.

Strazzulla G, Cooper JF, Christian ER, *et al.* (2003) Ion irradiation of TNOs: from the fluxes measured in space to the laboratory experiments. *C R Phys* 4:791–801.

Susi H and Ard JS (1971) Vibrational spectra of nucleic acid constituents. 1. Planar vibrations of uracil. *Spectrochim Acta A* 27:1549.

Trilling DE (2016) The surface age of Sputnik Planum, Pluto, must be less than 10 million years. *Plos One* 11:1–5.

Varghese AJ (1971) Photochemistry of uracil and uridine. *Biochemistry* 10:4283–4290.

Wang SY (1961) Photochemical reactions in frozen solutions. *Nature* 190:690–694.

Wang TF and Bowie JH (2012) Can cytosine, thymine and uracil be formed in interstellar regions? A theoretical study. *Org Biomol Chem* 10:652–662.

Ziegler JF, Ziegler MD, and Biersack JP (2010) SRIM—the stopping and range of ions in matter. *Nucl Instrum Methods Phys Res B* 268:1818–1823.

Address correspondence to:
Perry A. Gerakines
Astrochemistry Laboratory
NASA Goddard Space Flight Center
Greenbelt, MD 20771
USA

E-mail: perry.a.gerakines@nasa.gov

Submitted 12 April 2021
Accepted 20 September 2021
Associate Editor: Lewis Dartnell

Abbreviations Used

IR = infrared
ISM = interstellar medium